

BroadCAM: Outcome-agnostic Class Activation Mapping for Small-scale Weakly Supervised Applications

Jiatai Lin, Guoqiang Han, Xuemiao Xu, Changhong Liang, Tien-Tsin Wong, C. L. Philip Chen, Zaiyi Liu, Chu Han

Abstract—Class activation mapping (CAM), a visualization technique for interpreting deep learning models, is now commonly used for weakly supervised semantic segmentation (WSSS) and object localization (WSOL). It is the weighted aggregation of the feature maps by activating the high class-relevance ones. Current CAM methods achieve it relying on the training outcomes, such as predicted scores (forward information), gradients (backward information), etc. However, when with small-scale data, unstable training may lead to less effective model outcomes and generate unreliable weights, finally resulting in incorrect activation and noisy CAM seeds. In this paper, we propose an outcome-agnostic CAM approach, called BroadCAM, for small-scale weakly supervised applications. Since broad learning system (BLS) is independent to the model learning, BroadCAM can avoid the weights being affected by the unreliable model outcomes when with small-scale data. By evaluating BroadCAM on VOC2012 (natural images) and BCSS-WSSS (medical images) for WSSS and OpenImages30k for WSOL, BroadCAM demonstrates superior performance than existing CAM methods with small-scale data (less than 5%) in different CNN architectures. It also achieves SOTA performance with large-scale training data. Extensive qualitative comparisons are conducted to demonstrate how BroadCAM activates the high class-relevance feature maps and generates reliable CAMs when with small-scale training data.

Index Terms—Class Activation Mapping, Broad Learning System, Weakly Supervised Semantic Segmentation, Weakly Supervised Object Localization.

arXiv:2309.03509v1 [cs.CV] 7 Sep 2023

1 INTRODUCTION

CLASS activation mapping (CAM) [1] has attracted great attention and emerged significant advancements in the past few years. It was first proposed to visualize the regions where the classification models focus for interpretability. Lately, it has been widely adopted for weakly supervised applications to reduce annotation efforts by using only image-level labels to achieve dense pixel-level predictions, including weakly supervised semantic segmentation (WSSS) [2] and weakly supervised object localization (WSOL) [3].

Most of the existing WSSS and WSOL approaches rely on the training outcomes to construct the correlation between the feature maps and their correlated categories, such as gradients for Grad-CAM [4] and prediction scores for

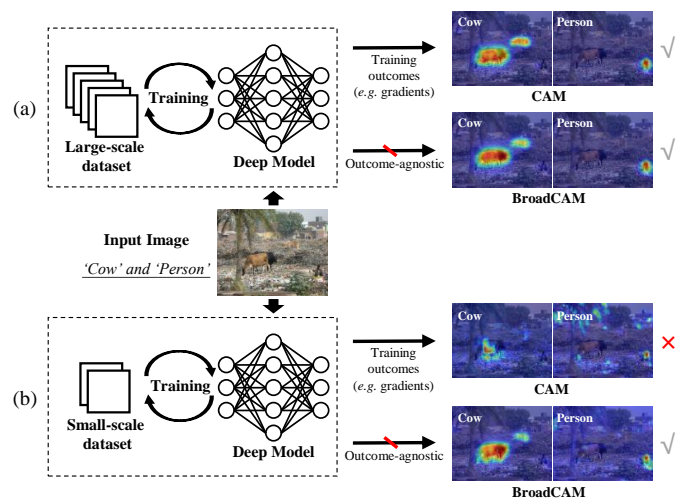


Fig. 1. Comparison with CAM and our BroadCAM on large-scale data (a) and small-scale data (b). Existing CAM approaches rely on the training outcomes, and achieve good results on large-scale data but noisy results on small-scale data. The proposed BroadCAM is capable of generating stable class activation maps for the models trained on both large- and small-scale datasets.

- Jiatai Lin, Guoqiang Han, Xuemiao Xu and C. L. Philip Chen are with the School of Computer Science and Engineering, South China University of Technology, Guangzhou, Guangdong, 510006, China.
- Changhong Liang, Zaiyi Liu and Chu Han are with Guangdong Provincial Key Laboratory of Artificial Intelligence in Medical Image Analysis and Application, Guangzhou 510080, China and the Department of Radiology, Guangdong Provincial People's Hospital (Guangdong Academy of Medical Sciences), Southern Medical University, Guangzhou 510080, China.
- Xuemiao Xu is with the School of Computer Science and Engineering at South China University of Technology, and also with State Key Laboratory of Subtropical Building Science, Ministry of Education Key Laboratory of Big Data and Intelligent Robot and Guangdong Provincial Key Lab of Computational Intelligence and Cyberspace Information.
- Tien-Tsin Wong is with the Department of Computer Science and Engineering, The Chinese University of Hong Kong, Hong Kong, China.
- Equal contribution: Jiatai Lin; Guoqiang Han.
- Corresponding author: Zaiyi Liu; Chu Han.

Score-CAM [5], and generate weights for the feature map aggregation. Thanks to the large-scale open source data in the community (e.g., ImageNet [6], [7] and COCO [8]), current CAM-based weakly supervised applications have achieved outstanding performance as shown in Fig. 1 (a). However, when with small-scale data, the model training

may become unstable, which leads to unreliable training outcomes and finally generates noisy weights. That is the reason why most of the current CAM approaches that depend on the training outcomes fail to generate reliable CAM seeds for weakly supervised applications, shown in Fig. 1 (b). And this situation cannot be underestimated. Because in the deep learning era, a tailored dataset for each specific task or scenario is indispensable, but most of the large-scale datasets were collected for the general natural scenes. Collecting massive well-labeled data from scratch is extremely difficult and labor-intensive. Therefore, a reliable approach for small-scale weakly supervised applications is crucial for reducing the cost and efforts of dense annotations and accelerating the annotation process.

Since the unreliable training outcomes are the reason why existing CAM approaches fail to generate appropriate CAM seeds with small-scale data. The most intuitive idea is to make the CAM generation process independent to the training outcomes. So the key problem to be solved is to re-construct the correlation between the feature maps and their correlated categories in an alternative way while ensuring the high and low class-relevance feature maps are activated and deactivated, respectively. To this end, we propose an outcome-agnostic CAM approach, called BroadCAM, for small-scale weakly supervised applications. Broad learning system (BLS) [9] is introduced as an independent classifier to re-construct the correlation. Thanks to the outcome-agnostic nature, BLS can avoid the weights being affected by the unreliable model outcomes while successfully activating the high class-relevance feature maps and deactivating the low class-relevance ones. Thanks to the robustness of BLS in handling small-scale data [10], the training of BLS is stable and the generated weights are more reliable when with insufficient training samples. To further bridge the gap between image-level labels and dense pixel-level predictions, we introduce more information by aggregating multi-layer feature maps. To the best of our knowledge, we are the first CAM approach to handle small-scale weakly supervised applications.

We conduct extensive experiments to evaluate the quality of CAM seeds for WSSS and WSOL on three datasets, including two natural image ones and a medical image one. Quantitative results demonstrate that BroadCAM greatly outperforms the most representative CAM methods across different model architectures and training strategies in small-scale data (less than 5%). In the entire data gamut experiments, the CAM seed generated by BroadCAM also consistently achieves state-of-the-art (SOTA) performance for both WSSS and WSOL on all the datasets. By qualitatively comparing with SOTA CAM approaches, BroadCAM is highly related to the corresponding categories with more complete activation and fewer noises when with small-scale training data. In the meanwhile, BroadCAM also shows superior activation results when with large-scale data. Furthermore, by visualizing the relationship between the weights and feature maps, we observe that BroadCAM activates more high class-relevance feature maps and fewer low class-relevance ones than conventional CAM approaches in small-scale data. To summarize, BroadCAM is an effective and flexible CAM approach for weakly supervised applications which is less susceptible to the dataset size. The contribu-

tions of this paper are summarized as follows.

- This paper is the first study that focuses on small-scale weakly supervised applications. We provide a feasible solution by making the CAM generation process independent to training outcomes when they are not reliable.
- We introduce a novel outcome-agnostic CAM named BroadCAM for small-scale WSSS and WSOL. BLS guarantees the reliability of the weights in small-scale data. Multi-layer feature map aggregation bridges the gap between weak supervision and dense prediction.
- Data gamut experiments on both WSSS and WSOL demonstrate the superiority and robustness of BroadCAM compared with the most representative CAM approaches. BroadCAM achieves SOTA quantitative performance in two natural image datasets and one medical image dataset.
- Qualitative comparisons demonstrate the robustness of BroadCAM on all datasets with small-scale data. Visualization of the relationship between CAM weights and feature maps shows the reliability of CAM weights generated by BroadCAM.

2 RELATED WORKS

2.1 CAM-based Weakly Supervised Applications

Weakly supervised applications, including WSSS and WSOL, leverage image-level labels to achieve dense pixel-level predictions [2], [3]. The major challenge is the huge information gap between weak supervision and dense prediction. Class activation mapping (CAM) technique [1] provides a feasible solution to overcome this challenge. Since the feature maps of the classification model are able to reveal the position and semantically related areas of the target classes. Therefore, CAM-based approaches have become the mainstream for weakly supervised applications.

Current WSSS and WSOL approaches apply various training strategies or introduce more useful information to push the classification task toward the segmentation/localization tasks. To avoid the classification model only focusing on the most distinguishable regions, the dropout strategy [11], [12] is introduced to deactivate the most discriminative areas, forcing the model to learn from non-predominant regions and generate more complete CAM seeds. To solve the incorrect activations in different scales, SEAM [13] is proposed to reconstruct the consistency over different rescaling transformations in a self-supervised manner. To encourage finer local details, PuzzleCAM [14] and L2G [15] are proposed to train the classification model jointly by the whole image and the cropped/tessellated images. To introduce additional object information, saliency-guided methods have been proposed to exploit the saliency maps as background cues [16], [17], pseudo-pixel supervision [18] and class-specific attention cues [19]. Moreover, existing studies also introduce information from other aspects to bridge the information gap, such as contrastive self-attention [20], data augmentation [21] and domain adaptation [22].

By reviewing CAM-based weakly supervised techniques, we find that current approaches are basically constructed on top of the deep models trained on large-scale training data. However, pursuing sufficient high-quality labeled data is labor-intensive, even for image-level labels. Although the foundation models are the trend of future artificial intelligence (AI) [23], the paradigm of current AI models remains one dataset for one specific task. Small-scale data will still be an inevitable problem for a long time in the deep learning era. Gao *et al.* [24] presents a pioneering study on large-scale unsupervised semantic segmentation (LUSS) with a released benchmark. However, even though they have achieved SOTA performance on LUSS, the precision of the results is still insufficient in practice due to the lack of supervision. In this paper, we first raise the importance of small-scale weakly supervised applications and propose a novel BroadCAM for them.

2.2 Class Activation Mapping (CAM)

Besides the training strategy, CAM techniques are also crucial for WSSS and WSOL. Essentially, CAM seed generation is a weighted aggregation of the feature maps. The quality of CAM seeds strongly relies on the robustness of the weights, which determine whether higher class-relevance feature maps (shown in Fig. 2) can contribute more activation. Current CAM methods generate weights by constructing the correlation between the feature maps and their corresponding categories based on the training outcomes, which can be categorized into two types: gradient-based and gradient-free methods.

2.2.1 Gradient-based CAM

GradCAM [4] is the first CAM approach that leverages gradient information to improve the flexibility of CAM, which has been widely applied to WSSS and WSOL. Later, various gradient-based methods have been proposed to improve the granularity by the smoothing technique, such as GradCAM++ [25], smooth GradCAM++ [26] and etc. To make the CAM seeds more complete for weakly supervised applications, LayerCAM [27] is proposed to introduce additional coarse-to-fine information by weighted aggregating multi-layer feature maps. BagCAM [28] identifies globally discriminative areas by deriving a set of regional localizers from the well-trained classifier, rather than solely activating regional object cues.

2.2.2 Gradient-free CAM

To avoid the saturation and false confidence problems of gradient, Score-CAM [5] utilizes forward information (predicted score) to replace backward information (gradient) to achieve less noisy CAM seeds. Lately, several score-based CAM methods have been introduced to advance Score-CAM to generate more complete visual explanations of deep models by the smooth operation (SS-CAM [29]) and integration operation (IS-CAM [30]). To produce high-quality and class-discriminative localization maps, Ablation-CAM [31] employs ablation analysis to measure the significance of individual feature map units to obtain the weights for CAM generation. Relevance-CAM [32] overcomes the shattered

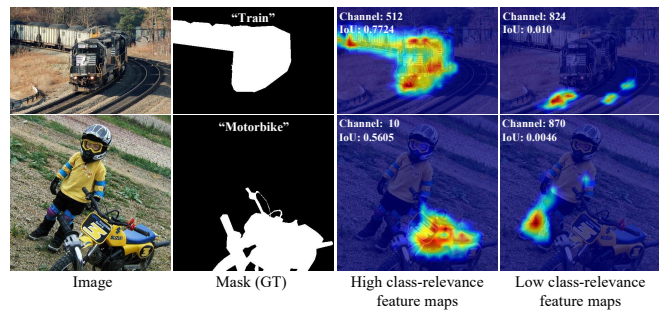


Fig. 2. Examples of high and low class-relevance feature maps. For each feature map, we calculate the IoU between the activated region (threshold: 0.1) and the ground truth mask to measure the relevance between each feature map and the corresponding category.

gradient problem at shallow layers by utilizing a relevance propagation process.

Although current CAM techniques bridge the gap between weak supervision and dense predictions, they are still based on an underlying assumption of the presence of large-scale data. When with small-scale data, the performance of current training outcome-based CAM methods may suffer from a dramatic decrease since unstable training will lead to unreliable training outcomes. To overcome such difficulty, we propose an outcome-agnostic CAM approach for small-scale data by breaking the dependency on training outcomes when generating CAM seeds.

2.3 Broad Learning System (BLS)

Broad learning system (BLS) [9], [33], [34] is a flat and lightweight classification network without the need for deep architecture. It constructs the correlation fleetly between the image/features and labels by feature mapping and enhanced mapping to avoid the retraining process. In the last few years, various modified BLS have been developed to improve the broad learning architecture and the feature mapping manner, such as Fuzzy-BLS [35], TDFW-BLS [36], stacked-BLS [37], Recurrent-BLS [38] and etc. BLS is also widely applied in various applications such as hyperspectral image classification [39] and micro-robotic control [40].

In our previous studies [10], [41], we also explore the capability of BLS on small-scale classification. Our proposed pyramidal deep-broad learning (PDBL) demonstrates more stable and superior performance in different CNN architectures compared with the conventional deep learning manner on small-scale data. Even if the model training is unstable with small-scale data, BLS can still successfully construct the correlation between the features and the labels. Therefore, we further extend BLS to the problem of small-scale CAM generation and finally empower small-scale WSSS and WSOL.

3 BROADCASTCAM

In this paper, we propose an outcome-agnostic CAM approach for small-scale WSSS and WSOL, called BroadCAM. Since CAM seed generation is essentially a weighted aggregation of the feature maps. Generating high-quality CAM seeds depends on whether CAM weights can activate

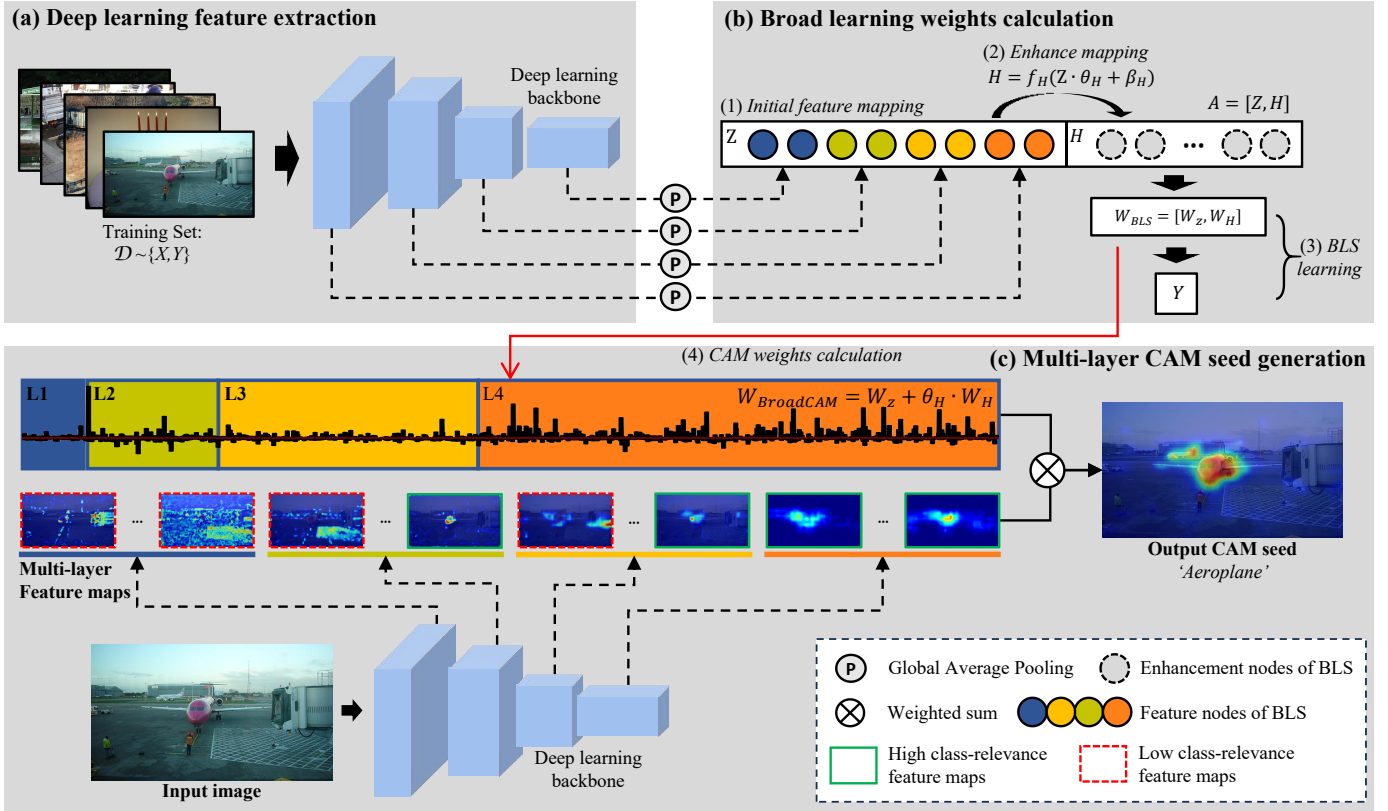


Fig. 3. The model framework of our proposed BroadCAM, which includes three steps. (a) Deep learning feature extraction: We first extract the features of multiple layers from a deep learning model. (b) Broad learning weights calculation: A broad learning system with only one-round learning is applied to generate the BroadCAM weights $W_{BroadCAM}$. (c) Multi-layer CAM seed generation: CAM seed is generated by a weighted aggregation of the multi-layer feature maps. We define the high class-relevance feature map as the one with a larger overlap with the ground truth label.

the higher class-relevance feature maps and deactivate the lower ones. For small-scale weakly supervised applications, outcome-based CAM approaches generally fail to generate reliable weights due to unstable training outcomes. Thus, we design a novel outcome-agnostic CAM approach by making the weights generation process independent of the training outcomes. Fig. 3 demonstrates the workflow of the proposed BroadCAM. And the details of BroadCAM are shown as follows.

3.1 Deep Learning Feature Extraction

Given a training set $\mathcal{D} \sim \{X, Y\}$, where X and Y are the training samples and the corresponding image-level labels, we first train a classification model f_{DL} to learn domain-specific knowledge from the dataset, just like the other CAM approaches. Then we use the classification model as the deep feature extractor. To further bridge the gap and introduce more information, we extract deep features from multiple layers.

$$\mathcal{F}_1, \mathcal{F}_2, \dots, \mathcal{F}_j = f_{DL}(x, \theta_{DL}) \quad (1)$$

where j is the index of the layers. $x \in X$, θ_{DL} and \mathcal{F}_j represent a sample x in the training set X , parameters of deep learning model and the feature maps of the j^{th} layer. Since the deep learning architecture in BroadCAM only serves for feature extraction. Any training strategy to

enhance the feature maps can be applied to this framework. And we will discuss this in the experiments.

3.2 Broad Learning Weights Calculation

Next, we construct the correlation between the deep features and the corresponding categories and generate the weights for each feature map. Inspired by our previous studies [10], [41], a broad learning system (BLS) is a lightweight and flat architecture that is a robust classifier for small-scale data. Thus, we introduce BLS to generate CAM weights for CAM seed generation. In the BLS, we first map the deep feature maps to broad features to fit the broad learning architecture by initial feature mapping. Then, we establish the enhancement nodes to expand the feature broadly by enhanced mapping. And we solve the optimization problem of BLS with extended broad learning feature nodes by ridge regression algorithm. Finally, we can transform the BLS parameters to obtain the weights for CAM seed generation.

(1) Initial Feature Mapping: For the feature maps \mathcal{F}_j extracted from the j^{th} layer, we first apply global average pooling (GAP) f_{GAP} to squeeze the deep learning features by:

$$z_j = f_{GAP}(\mathcal{F}_j) \quad (2)$$

where z_j represents the squeezed features of the j^{th} layer. Then we concatenate the multi-layer features of each sample

into a broad feature vector \mathbf{z} as the feature node to fit the BLS architecture:

$$\mathbf{z} = [z_1, z_2, \dots, z_j]^T. \quad (3)$$

We form a broad feature matrix Z of all the training samples by:

$$Z = [\mathbf{z}^1, \mathbf{z}^2, \dots, \mathbf{z}^i]^T \quad (4)$$

where i is the index of samples.

(2) Enhance Mapping: Next, we perform an enhanced mapping on the feature nodes to expand the broad structure widely and improve the BSL optimization.

$$H = f_H(Z \times \theta_H + \beta_H). \quad (5)$$

where f_H is a linear activation function. θ_H and β_H represent the weights and bias of enhance mapping. θ_H is used to group the feature nodes with similar importance. Different from the original BLS design with randomly initialized weights θ_H , θ_H is now initialized by the class-relevance of the features Z . To acquire the class relevance, we first solve BLS using the initial feature nodes to calculate the parameters W_{init} by:

$$W_{init} = (\lambda I + ZZ^T)^{-1} Z^T Y \quad (6)$$

where I and λ denote the unit matrix and the hyper-parameter of the L2 norm constraint for W_{init} . Then we use W_{init} to initialize θ_H .

(3) BLS Learning: Then we utilize all the broad features to learn BLS to construct the relationship between the features and the corresponding image-level labels Y . We first concatenate the feature nodes and enhancement nodes together into an expanded broad feature matrix, denoted as $A = [Z, H]$. Next, we employ the ridge regression algorithm to calculate the parameters of BLS as follows:

$$W_{BLS} = (\lambda I + AA^T)^{-1} A^T Y \quad (7)$$

where W_{BLS} is the BLS parameters which can be split into two parts W_Z and W_H for the feature nodes and enhancement nodes, respectively.

(4) CAM Weights Calculation: To use the BLS parameters to generate the CAM weights for each feature map, we transform the formulation of BLS as follows:

$$\begin{aligned} Y &= A \cdot W_{BLS} = [Z, H] \times [W_Z, W_H]^T \\ &= Z \times W_Z + H \times W_H \\ &= Z \times W_Z + (Z \times \theta_H + \beta_H) \times W_H \\ &= Z \times (W_Z + \theta_H \times W_H) + \beta_H \times W_H \end{aligned} \quad (8)$$

$$\text{denote} := Z \times W_{BroadCAM} + \sigma$$

where $\sigma = \beta_H \times W_H$ is the bias of the BLS and $W_{BroadCAM} = W_Z + \theta_H \times W_H$ represents the weights that directly connect the feature nodes to the predicted classification results, quantifying the relevance between deep feature maps and categories. Since each value of the broad feature vector Z is calculated by GAP from the corresponding deep feature map of F . The CAM weights of Z are equivalent to the CAM weights of F . It is the channel-wise weights utilized for aggregating feature maps to generate class activation maps.

TABLE 1
Data distribution of VOC2012, BCSS-WSSS and OpenImages30k datasets.

Task	Dataset	Num. of categories	Num. of samples		
			train	val	test
WSSS	VOC2012 [42]	20	10,582 (aug)	1,449	1,456
	BCSS-WSSS [12]	4	23,422	3,418	4,986
WSOL	OpenImages30k [43], [44]	100	29,819	2,500	5,000

3.3 Multi-layer CAM Seeds Generation

Finally, we can use $W_{BroadCAM}$ to generate CAM seeds in the weights aggregation manner by:

$$M_{BroadCAM} = ReLU([\mathcal{F}_1, \mathcal{F}_2, \dots, \mathcal{F}_i] \times W_{BroadCAM}) \quad (9)$$

where $ReLU$ is the non-linear activation function. The proposed BroadCAM can aggregate the feature maps from multiple layers.

4 DATASETS

In this paper, we evaluate the proposed BroadCAM on three datasets including the VOC2012 dataset (WSSS), BCSS (WSSS), and OpenImages30k (WSOL), which are detailed in this section. The distributions of three datasets are demonstrated in Table 1.

4.1 VOC2012 Dataset

VOC2012 dataset¹ is the standard dataset provided by The PASCAL Visual Object Classes Challenge [42], which has been used for weakly supervised semantic segmentation (WSSS) tasks in recent years. VOC2012 dataset comprises 20 foreground categories, encompassing Car, Bus, Bicycle, etc. It can be split into training set (1464 images), validation set (1449 images) and test set (1456 images). Following the previous WSSS study [14], the training set has been extended to an augmented training set which includes 10,582 training samples. Image-level labels are provided for model training and pixel-level annotations are for evaluation. In our experiments, we use the augmented training set with different proportions to train the models and evaluate the CAM seed in the original training set and validation set.

4.2 BCSS-WSSS Dataset

Breast Cancer Semantic Segmentation (BCSS) dataset [45]² is a well-labeled dataset for histopathological tissue semantic segmentation task of breast cancer. It consists of 151 representative regions of interest (ROIs) which were selected from 151 whole slide images (WSIs) and labeled by pathologists, pathology residents, and medical students. In this dataset, pixel-level annotations were provided for fully supervised model training, including 4 predominant classes (e.g., tumor, stroma, lymphocyte-rich regions and necrosis.), 6 non-predominant classes (e.g., artifacts, blood,

1. <http://host.robots.ox.ac.uk/pascal/VOC/voc2012/>
2. <https://bcsegmentation.grand-challenge.org/>

TABLE 2

Comparison of our proposed BroadCAM and existing CAM approaches on VOC2012 and BCSS-WSSS datasets with different proportions of training data. mIoU and FwIoU are used for the evaluation of VOC2012 and BCSS-WSSS, respectively. **Bold** represents the best performance.

Dataset	Training strategy (Architecture)	Split	CAM method	Performance of CAM seeds with different proportions of training samples								
				1%	2%	5%	8%	10%	20%	50%	80%	100%
VOC2012 (natural image)	Puzzle [14] (ResNeSt101)	train	CAM	34.13	37.18	46.51	47.44	49.75	53.55	58.15	58.89	59.55
			GradCAM	33.89	36.71	46.05	47.05	49.40	53.10	57.82	58.85	59.53
			LayerCAM	41.18	43.46	46.27	47.03	49.54	45.61	51.18	54.12	54.64
			BroadCAM	46.45	47.02	48.57	49.55	51.51	54.22	55.90	58.39	58.52
		val	CAM	33.85	36.83	46.28	47.00	49.41	53.58	57.33	58.99	59.00
			BroadCAM	46.55	46.78	48.54	49.18	51.23	53.78	54.72	57.33	57.41
	Puzzle [14] (ResNeSt269)	train	CAM	30.11	38.59	45.25	51.55	51.17	54.26	56.66	58.89	58.85
			GradCAM	29.97	37.92	44.58	50.62	50.04	53.93	56.02	58.53	58.47
			LayerCAM	41.81	44.52	45.88	50.60	48.85	53.12	52.89	55.01	55.47
			BroadCAM	49.37	49.00	49.78	54.38	52.26	57.03	56.85	58.69	57.89
		val	CAM	29.95	38.96	44.85	51.53	51.56	54.27	56.11	58.39	58.45
			BroadCAM	49.87	48.31	49.63	54.06	52.17	56.20	56.67	57.96	57.49
BCSS-WSSS (medical image)	PDA [12] (ResNet38)	val	CAM	48.38	60.17	65.91	68.24	69.18	69.55	69.69	70.11	70.64
			GradCAM	48.37	59.81	65.96	68.30	69.28	69.87	69.85	70.32	70.79
			LayerCAM	52.93	64.46	65.92	66.86	67.35	68.90	69.51	69.04	68.78
			BroadCAM	59.92	64.77	66.86	69.01	68.11	71.73	71.03	71.08	71.54
		test	CAM	55.91	67.53	71.80	73.71	73.44	73.04	73.18	73.93	74.14
			GradCAM	55.84	67.43	72.09	73.98	73.69	73.38	73.37	74.13	74.26
			LayerCAM	59.09	67.64	68.90	69.78	70.08	71.11	71.72	71.46	70.84
			BroadCAM	66.63	70.50	71.79	74.09	72.41	74.59	74.14	74.47	74.93

etc.) and 8 challenging classes (e.g. plasma cells, lymph vessels, etc.)

Based on the BCSS dataset, our previous study [12] recreates a new dataset (BCSS-WSSS dataset) for weakly supervised semantic segmentation, which cropped the patches from original ROIs and obtained the corresponding image-level labels from the pixel-level annotations. In the BCSS-WSSS dataset, 4 foreground categories were defined based on the predominant classes of the BCSS dataset, including Tumor (TUM), Stroma (STR), Lymphocytic infiltrate (LYM), Necrosis (NEC).

4.3 OpenImages30k Dataset

OpenImages30k dataset [43], [44]³ is curated for weakly supervised object localization (WSOL) task based on the OpenImagesV5 dataset [46]⁴. It consists 100 categories with balanced number of samples in each category. Samples of OpenImages30k were selected randomly from the OpenImagesV5 dataset which can be split into training set (29819 images), validation set (2500 images) and test set (5000 images), respectively. In this dataset, the image-level labels are provided in the training set for classification model training with different proportions and pixel-level annotations were created for evaluation.

5 EXPERIMENTS

In this section, we first show the evaluation metrics in our experiments in Section 5.1. Then, we evaluate the quality of the CAM seeds generated by various CAM techniques on both WSSS and WSOL in three datasets in Section 5.2 and

Section 5.3. Next, we comprehensively analyze the reliability of the CAM weights in Section 5.4. Finally, we conduct an ablation study on the multi-layer design of BroadCAM in Section 5.5.

5.1 Evaluation Metrics

In this paper, we conduct the comparison of CAM methods on VOC2012 dataset [42] (WSSS, natural image), BCSS-WSSS [12] (WSSS, medical image) and OpenImages30k [43], [44] (WSOL, natural image), respectively. We employ three metrics to evaluate the performance of CAM seeds:

- mIoU: We first employ the Mean Intersection over Union (mIoU) metric to evaluate the performance on the VOC2012 dataset for the WSSS task of natural image. We use a range of thresholds to quantify the mIoU of CAM seeds separately and record the peak one representing the performance of CAM methods.
- FwIoU: Following the setting of our previous study [12], we utilize the Frequency weighted Intersection over Union (FwIoU) metric to evaluate the performance of CAM methods on BCSS-WSSS dataset.
- mPxPA: In the experiments on OpenImages30k dataset (natural image), we utilize the mean pixel average precision (mPxAP) [43], [44] metric to quantify the performance of CAM methods for WSOL task.

5.2 Comparisons of CAM Methods on WSSS

First of all, we compare our BroadCAM with three representative CAM methods on WSSS, including the original CAM [1] and two gradient-based CAM approaches (GradCAM [4] and LayerCAM [27]). All the experiments are conducted on a natural image dataset VOC2012 [42]

³ <https://github.com/clovaai/wssolevaluation>

⁴ https://storage.googleapis.com/openimages/web/download_v5.html

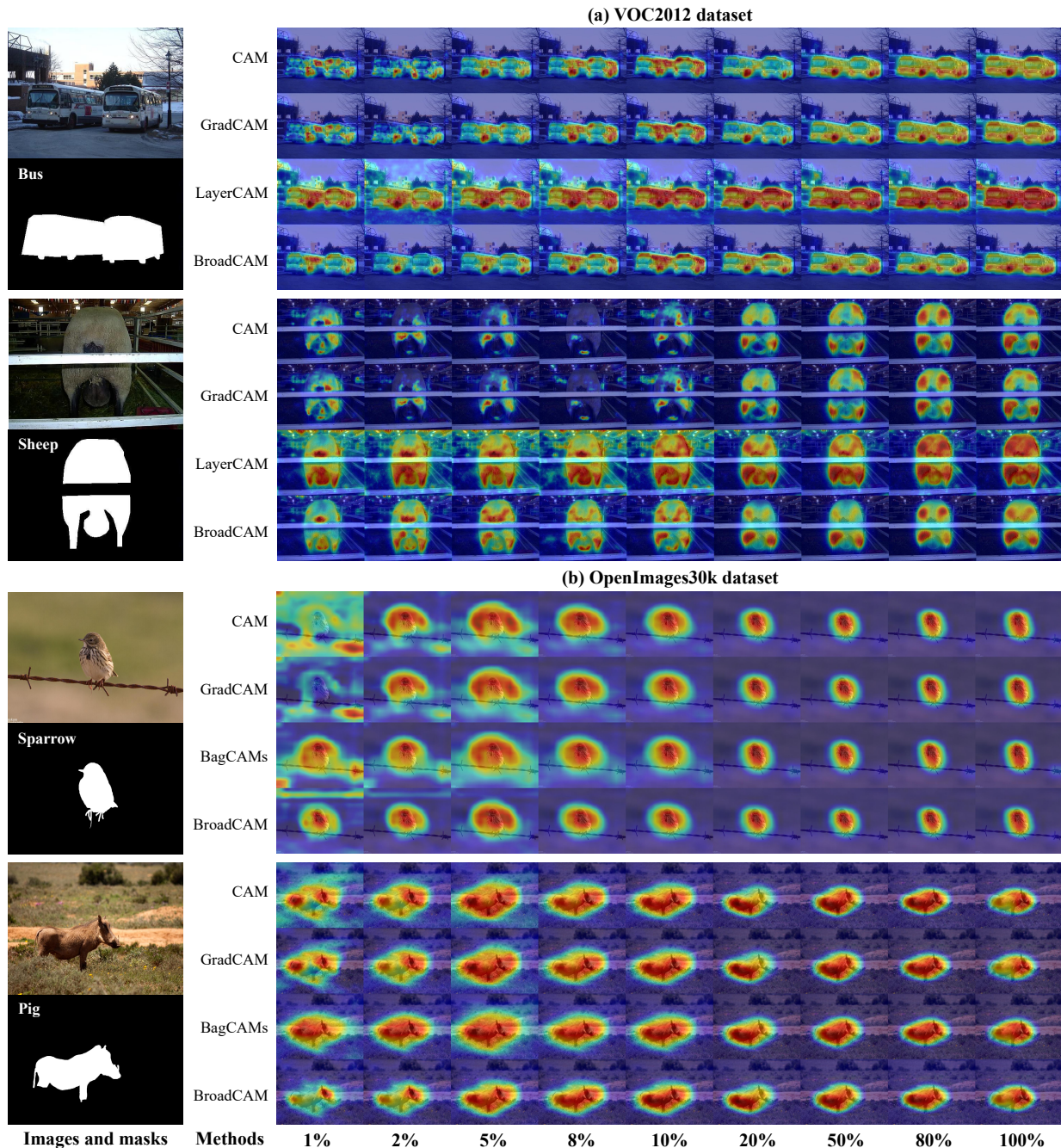


Fig. 4. Comparison with CAM seeds generated by CAM methods (CAM, GradCAM, LayerCAM, BagCAM and our BroadCAM) with models trained on training set of different proportions on VOC2012 dataset and OpenImages30k dataset. Horizontally: 1st column represents the original image and mask. Then the next 9 columns are the CAM seeds generated with models trained on training sets of different proportions (1%, 2%, 5%, 8%, 10%, 20%, 50%, 80%, 100%), respectively.

and a medical image dataset BCSS-WSSS [12]. To comprehensively investigate the performance of CAM approaches from large-scale data to small-scale data, we conduct a data gamut experiment with different proportions of the training data (1%, 2%, 5%, 8%, 10%, 20%, 50%, 80%, 100%). Besides the scale of the data, we also conduct comparisons on various CNN architectures and training strategies. For the experiments on the VOC2012 dataset, we employ the puzzle strategy proposed in PuzzleCAM [14] on ResNeSt101 and ResNeSt269 [47], respectively. For the experiment on the BCSS-WSSS dataset, we apply our previously pro-

posed training strategy, called progressive dropout attention (PDA) [12], on ResNet38 [48]. Since we only evaluate the quality of the CAM seeds in this experiment, we do not apply any post-processing step, like AffinityNet [49] and IRNet [50], or second-round training by the pseudo masks. Note that, no matter how many training samples are used to train the classification model, the evaluations are performed under the entire training, validation and test sets.

Table 2 demonstrates the quantitative results of different approaches to WSSS on two datasets. We can observe that CAM seeds generated by all the CAM methods with large-

TABLE 3

Comparison of our proposed BroadCAM and existing CAM approaches on OpenImages30k dataset with different proportions of training data. mPxAAP is used for the evaluation.

Dataset	Training strategy (Architecture)	Split	CAM method	Performance of CAM seeds with different proportions of training samples								
				1%	2%	5%	8%	10%	20%	50%	80%	100%
OpenImages30k (natural image)	DA-WSOL [22] (ResNet50)	val	CAM	39.32	50.13	49.81	60.10	60.87	62.32	64.91	65.41	65.74
			GradCAM	43.38	53.67	51.44	61.92	62.73	63.89	66.42	66.98	67.64
			BagCAM	50.85	57.10	53.30	61.92	62.08	62.76	65.82	66.33	67.52
			BroadCAM	53.31	58.75	58.01	63.78	64.25	65.18	67.32	67.60	68.32
		test	CAM	38.47	49.41	49.57	59.54	60.35	61.50	64.07	64.68	65.05
			GradCAM	42.63	53.00	51.24	61.32	62.00	63.26	66.02	66.63	67.12
			BagCAM	49.54	56.29	52.64	60.84	61.38	62.01	65.45	65.78	66.89
			BroadCAM	52.71	58.68	57.48	63.32	63.86	65.01	67.16	67.51	68.10

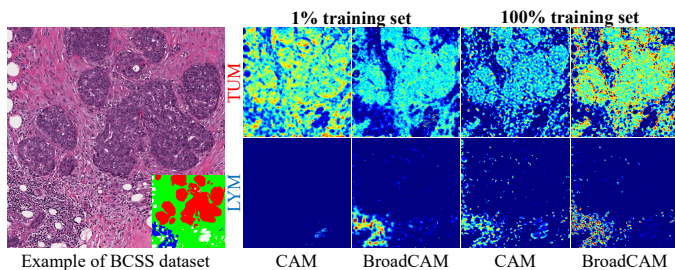


Fig. 5. Visual comparison of the CAM seeds generated by CAM and our BroadCAM. An example image and its ground truth are shown on the left-hand side (Red: tumor epithelium, Blue: lymphocyte, Green: stroma). On the right side, we show the CAM seeds of two classes TUM and LYM generated by CAM and BroadCAM with 1% and 100% training sets.

scale training data (more than 50%) exhibit exceptional performance in the VOC2012 dataset on both ResNeSt101 and ResNeSt269 architectures. Visualization in Fig. 4 (a) demonstrates that CAM, GradCAM and BroadCAM generate very similar CAM seeds when with large-scale data. Although LayerCAM provides high activation on the object, multi-layer design may also introduce more noisy activation. When the proportion of the training data decreases, the model training and the outcomes become less reliable. Therefore, the performance of outcome-based CAM approaches drops dramatically. Under the same experimental setting, we can observe that BroadCAM mitigates the performance degradation and constantly outperforms the outcome-based CAM approaches. For example, the performance of CAM seeds generated by the original CAM (ResNeSt269) on the validation set drops from 58.45 to 29.95, but BroadCAM can still achieve 49.87. Thanks to the outcome-agnostic nature, BroadCAM will not be affected by unreliable training outcomes and only focus on the relevance between the feature maps and the corresponding categories, leading to less noisy CAM seeds. As shown in Fig. 4 (a), outcome-based approaches show either incomplete or noisy activation. However, the CAM seeds generated by BroadCAM also show weaker activation on small-scale data than the ones on large-scale data. They are still more complete with less noise compared with the other three competitors.

To further evaluate the CAM seeds, we conduct an experiment on a medical image dataset, BCSS-WSSS. The training strategy, progressive dropout attention (PDA), applied in this experiment is proposed by our previous

study [12] to prevent the classification model from focusing on the most discriminative areas. As shown in the lower part of Table 2, BroadCAM almost dominates the entire data gamut experiment. Although the performance of all four CAM approaches decreases when reducing the training samples, BroadCAM still greatly outperforms the other three competitors. Fig. 5 demonstrates an example and the corresponding CAM seeds generated by the original CAM and BroadCAM on both 1% and 100% training sets. When the classification model is trained on the complete dataset, both CAM and BroadCAM can generate favorable CAM seeds. However, when the training set downscales to only 1%, conventional CAM fails to activate lymphocytes and generates noisy tumor CAM seeds. Thanks to the outcome-agnostic design, BroadCAM is able to generate high-quality CAM seeds with more complete and less noisy activation even if the training process is unstable.

5.3 Comparisons of CAM Methods on WSOL

Next, we conduct experiments to evaluate the ability of different CAM approaches on WSOL, including CAM [1], GradCAM [4], BagCAM [28] and BroadCAM. In this experiment, we employ the training strategy DA-WSOL [22] to train the ResNet50 model on different proportions of the training set in the OpenImages30k dataset. Quantitative results shown in Table 3 demonstrate that the CAM seeds generated by BroadCAM are well-qualified for object localization. A similar trend in WSSS results can also be observed in WSOL ones that the performance of BroadCAM decreases more smoothly than existing CAM approaches along with the reduction of training data. Fig. 4 (b) visualizes CAM seeds generated by different CAM approaches with different training data scales. When with enough training data, there is no visual difference in all the CAM approaches. When reducing the training samples, existing outcome-based CAM approaches introduce false positive activation even the object can be easily separated from the background, such as the sparrow example.

To further evaluate the robustness and the flexibility of various CAM approaches on different WSOL training strategies, including original CAM [1] with no training strategy, ADL [11], cutmix [21] and DA-WSOL [22]. This experiment is conducted on 1% and 100% training sets. There is an interesting observation that not all the strategies proposed for WSOL can gain improvement compared with the original CAM baseline, which is also reported in the previous study [44]. Nevertheless, BroadCAM constantly

TABLE 4

Compared with the performance (mPxAP) of CAM seeds generated by CAM methods on models trained using different WSOL methods with a training set of different proportions on OpenImages30k dataset.

Dataset	Proportion	CAM methods	CAM [1]		ADL [11]		Cutmix [21]		DA-WSOL [22]	
			val	test	val	test	val	test	val	test
OpenImages30k (WSOL)	1%	CAM	38.05	37.09	32.71	31.64	37.35	36.27	39.32	38.47
		GradCAM	41.27	40.51	35.20	33.84	40.66	39.85	43.38	42.63
		BagCAM	47.47	46.19	38.39	37.04	46.74	45.40	50.85	49.54
		BroadCAM	51.88	51.24	48.73	47.58	51.23	50.55	53.31	52.71
	100%	CAM	58.50	57.85	56.78	56.37	57.31	56.27	65.74	65.05
		GradCAM	59.71	59.12	57.83	57.36	58.65	57.87	67.64	67.12
		BagCAM	60.01	59.33	57.94	57.48	59.04	58.06	67.52	66.89
		BroadCAM	62.23	61.68	60.61	60.25	61.89	61.15	68.32	68.10

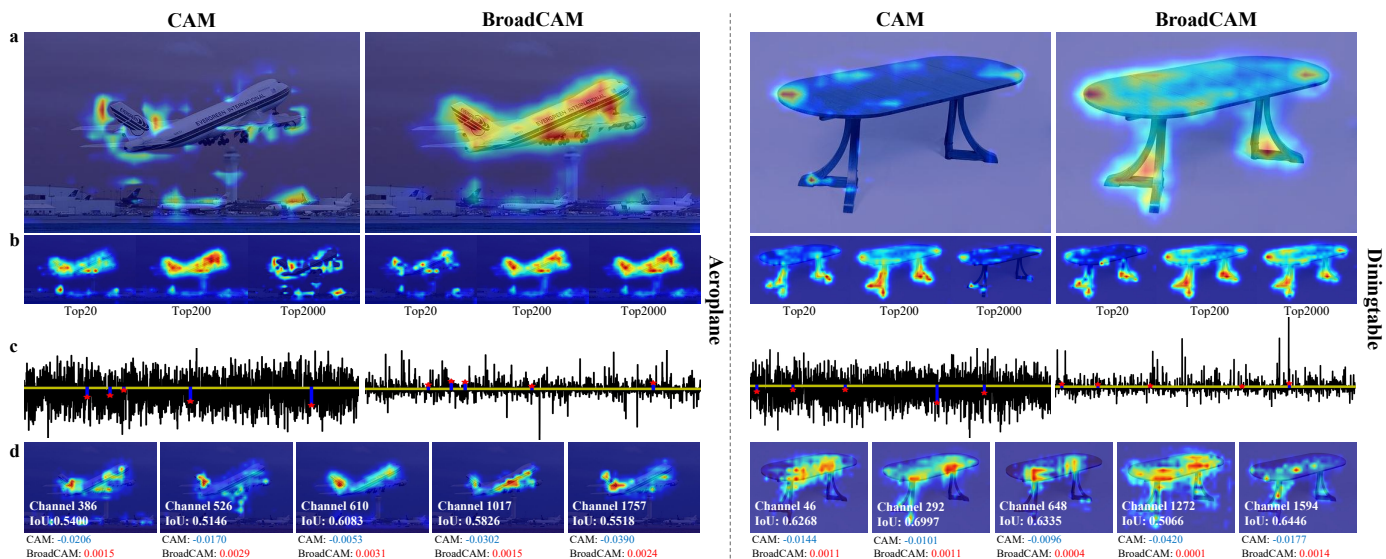


Fig. 6. Visual comparison of the reliability of CAM weights. Two examples are selected from the VOC2012 dataset and the experiment is conducted on 1% training set. (a) The CAM seeds generated by all the feature maps. (b) The CAM seeds generated by the selected feature maps of top20, top200, and top2000 weights. (c) The CAM weights in the order of the channel numbers of the feature maps, with five selected ones highlighted by red stars. (d) The selected feature maps and their corresponding channel number, IoU with ground truth and the value of the weights. Positive weights are marked in red and negative ones are marked in blue.

outperforms existing CAM approaches in all the training strategies. And the performance gap of BroadCAM between 1% and 100% training sets is the least among all the four CAM methods.

5.4 Reliability of CAM Weights

Since the CAM seeds are generated by the weighted linear aggregation of the feature maps. Therefore, whether the CAM weights are reliable will be the key to CAM generation. In this part, we conduct two visualization experiments to deeply investigate the reliability of the CAM weights, especially for small-scale data.

In the first experiment, we want to decode the relationship between the CAM weights and the feature maps. Fig. 6 (a) demonstrates two examples of CAM seeds generated by CAM and BroadCAM with a model trained on 1% training set. We can observe that the traditional CAM fails to generate reliable CAM seeds, whereas our BroadCAM succeeds. To explain this, we first generate three CAM seeds using the selected feature maps of top20, top200 and top2000 weights. In Fig. 6 (b), we can observe that the top20 and top200 results of CAM and BroadCAM are very similar. And both CAM seeds generated by the feature maps with

top200 weights can actually provide precise activation on the objects. However, in the top2000 results, we can observe an obvious activation degradation on the CAM seeds generated by the original CAM. This is because unreliable training with small-scale data will generate noisy weights for the outcome-based CAM techniques, leading to incorrect deactivation on the high class-relevance feature maps. To further justify this conclusion, we plot the CAM weights in Fig. 6 (c) and show five high class-relevance feature maps and their corresponding weights in Fig. 6 (d). Note that, the weights are in order of the channel numbers of the feature maps. We can easily observe that the original CAM deactivates the high class-relevance feature maps with negative weights, whereas BroadCAM activates them with positive weights. From this experiment, we make an assumption that the weights of BroadCAM have a higher correlation with the relevance (IoU) of feature maps when with small-scale data, compared with the original CAM.

To further investigate this assumption, we conduct another experiment to visualize the relationship between the distribution of CAM weights and the class-relevance feature maps. Fig. 7 demonstrates two examples with the generated CAM seeds on 1% and 100% training data. The line chart

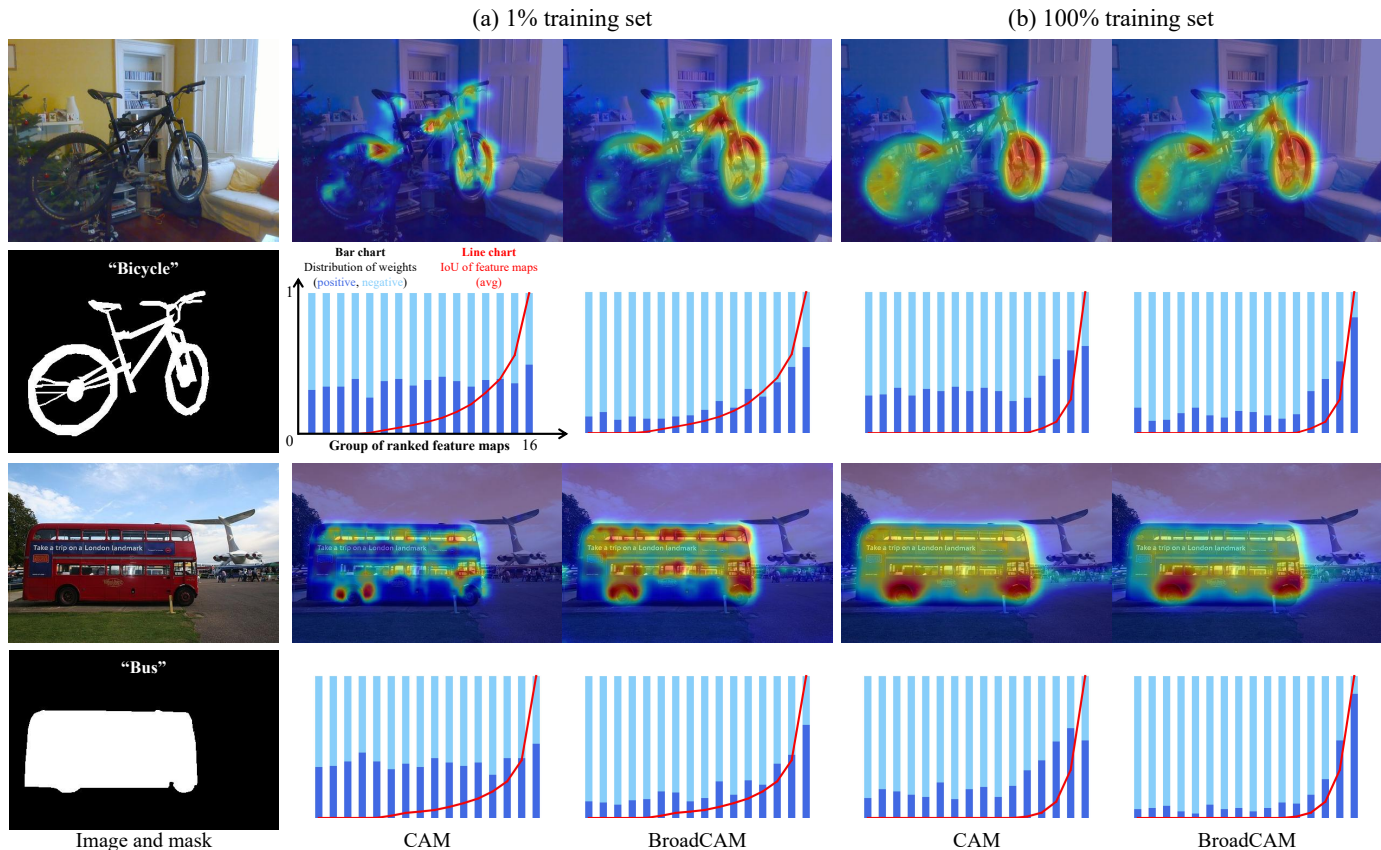


Fig. 7. Visualization of the relationship between the distribution of weights and the relevance of feature maps. Two examples are selected from the VOC2012 dataset and the experiment is conducted on both 1% and 100% training sets. For each example, we show the original image, pixel-level ground truth, generated CAM seeds and mixed charts with line charts and bar charts. In each mixed chart, we first group the feature maps according to the rank of the IoU. The line chart (in red) shows the IoU of each group of feature maps and the bar chart (in blue) demonstrates the distribution of the weights in each group. The number of positive/negative weights is in deep/light blue.

(in red) shows the IoU of the feature maps and the bar chart (in blue) demonstrates the distribution of the weights. The details of the experimental settings are demonstrated as follows. In the line chart, we first rank the feature maps by the IoU of the target class. Then we split the feature maps into 16 groups, each of which contains an equal number of feature maps. The red line is the average normalized IoU of each group of feature maps. In the bar chart, each bar indicates the total number of positive or negative weights in one group of feature maps. In each group, positive weights are in deep blue and negative weights are in light blue. By putting the bar chart and line chart together, we can easily observe that the weights generated by BroadCAM show more similar trends with the class relevance of the feature maps compared with the original CAM. For the cases in 100% training set in Fig. 7 (b), the number of positive weights is positively correlated with the class relevance for both BroadCAM and CAM, leading to favorable CAM seeds for both CAM techniques. However, when with only 1% training data in Fig. 7 (a), CAM fails to show a positive correlation but the one of BroadCAM still remains. Inaccurate activation makes CAM fail to generate clean and robust CAM seeds. This experiment somehow justifies our assumption that the weights generated by BroadCAM have a higher correlation with the relevance of feature maps compared with the original CAM, especially for small-scale

data, thanks to the outcome-agnostic nature.

5.5 Ablation Study on Multi-layer Design

Since BroadCAM is also capable of aggregating features from multiple layers. Here, we conduct an ablation study to discuss the advantages and drawbacks of the multi-layer design for BroadCAM in large-scale and small-scale weakly supervised applications. In this experiment, we train ResNeSt101 on 1% and 100% training sets of the VOC2012 dataset with different combinations of the layers in WSSS. L1 to L4 are from shallower layers to deeper layers. Quantitative results are shown in Table 5.

We first evaluate the performance of BroadCAM on the single layer. We can observe that using the feature maps extracted from the deepest layer shows the best performance as expected. Because the deeper layers deliver more semantic information and the shallow feature maps capture more textural information. When with a small-scale dataset, the feature maps are less stable and informative than with large-scale data, resulting in a significant decline in performance. Next, to evaluate the multi-layer performance, we gradually equip the other three layers on the deepest layer L4. Experimental results show that associating the last two layers achieves the best performance in both 1% and 100% training sets. When with large-scale data, the performance of BroadCAM on all the multi-layer configurations is

TABLE 5
Ablation study on multi-layer of BroadCAM in WSSS with 1% and 100% training set on VOC2012 dataset (mIoU).

Setting	1% training set		100% training set	
	train	val	train	val
L1	17.61	17.75	21.00	20.65
L2	22.47	22.35	26.50	26.23
L3	40.42	40.26	58.03	56.16
L4	45.79	46.21	58.17	57.30
L3+L4	46.02	46.40	58.76	57.55
L2+L3+L4	45.11	45.57	58.56	57.36
L1+L2+L3+L4	44.49	44.76	58.54	57.35

similar. However, when with small-scale data, introducing shallow layers will harm the CAM generation due to the unstable feature maps. In this paper, all the experiments are conducted using the BroadCAM with the last two layers (L3+L4).

6 CONCLUSION

In this paper, we first raise the importance of small-scale weakly supervised semantic segmentation and object localization, and propose a novel outcome-agnostic CAM method, called BroadCAM. To avoid the CAM weights being affected by unreliable outcomes due to unstable training, we introduce an independent broad learning system, which is friendly to small-scale data, to generate reliable CAM weights. Extensive quantitative and qualitative experiments on WSSS and WSOL tasks on three different datasets have proven the effectiveness and robustness of BroadCAM on both large-scale and small-scale data, whereas the existing CAM approaches are not able to achieve both. Two well-designed visualization experiments demonstrate that the outcome-agnostic design encourages BroadCAM to correctly activate more high class-relevance feature maps, resulting in less noisy and more complete CAM seeds. And the weights generated by BroadCAM are highly correlated with the relevance of the feature maps, which is the major reason why BroadCAM achieves more favorable results even when the training is unstable with small-scale data.

Since this study is the first one tailored for small-scale weakly supervised applications, and BroadCAM is the first outcome-agnostic CAM approach. We think that there exists a lot of future directions to be explored. (1) The reliability of the feature maps. In this study, we only focus on how to avoid the CAM weights being affected by unreliable training outcomes. However, unstable training will also harm the robustness of the feature maps when generating CAM seeds. Therefore, how to improve the feature representation ability for small-scale data is equally important. (2) How to make good use of shallow layers. Although BroadCAM leverages multi-layer information to generate CAM seeds. It still mainly relies on the deeper layers with more semantic information. However, the activation of the feature maps from deeper layers is coarse and more abstract. To introduce the finer details of the object boundaries, making good use of shallow layers might be a feasible solution.

As the first baseline model on small-scale weakly supervised applications, we hope BroadCAM can bring some insights to this field and encourage more studies to discover

more outstanding techniques to reduce the annotation efforts on semantic segmentation and object localization.

ACKNOWLEDGMENTS

This work was supported by the Key-Area Research and Development Program of Guangdong Province, China (No. 2021B0101420006), the Natural Science Foundation for Distinguished Young Scholars of Guangdong Province (No. 2023B1515020043), the National Science Foundation for Young Scientists of China (No. 62102103), the National Natural Science Foundation of China (No. 82372044, 82071892, 92267203 and 82271941), Regional Innovation and Development Joint Fund of National Natural Science Foundation of China (No.U22A20345), High-level Hospital Construction Project (No.DFJHBF202105), Guangdong Provincial Key Laboratory of Artificial Intelligence in Medical Image Analysis and Application (No. 2022B1212010011), the Science and Technology Major Project of Guangzhou (No. 202007030006), the Program for Guangdong Introducing Innovative and Entrepreneurial Teams (No. 2019ZT08X214), Key-Area Research and Development Program of Guangzhou City (202206030007). The source code of BroadCAM is available at <https://github.com/linjiatai/BroadCAM>.

REFERENCES

- [1] B. Zhou, A. Khosla, A. Lapedriza, A. Oliva, and A. Torralba, "Learning deep features for discriminative localization," in *2016 IEEE Conference on Computer Vision and Pattern Recognition (CVPR)*, 2016, pp. 2921–2929.
- [2] W. Shen, Z. Peng, X. Wang, H. Wang, J. Cen, D. Jiang, L. Xie, X. Yang, and Q. Tian, "A survey on label-efficient deep image segmentation: Bridging the gap between weak supervision and dense prediction," *IEEE Transactions on Pattern Analysis and Machine Intelligence*, pp. 1–20, 2023.
- [3] D. Zhang, J. Han, G. Cheng, and M.-H. Yang, "Weakly supervised object localization and detection: A survey," *IEEE Transactions on Pattern Analysis and Machine Intelligence*, vol. 44, no. 9, pp. 5866–5885, 2022.
- [4] R. R. Selvaraju, M. Cogswell, A. Das, R. Vedantam, D. Parikh, and D. Batra, "Grad-CAM: Visual explanations from deep networks via gradient-based localization," *International Journal of Computer Vision*, vol. 128, no. 2, pp. 336–359, oct 2019.
- [5] H. Wang, Z. Wang, M. Du, F. Yang, Z. Zhang, S. Ding, P. Mardziel, and X. Hu, "Score-cam: Score-weighted visual explanations for convolutional neural networks," in *Proceedings of the IEEE/CVF conference on computer vision and pattern recognition workshops*, 2020, pp. 24–25.
- [6] J. Deng, W. Dong, R. Socher, L.-J. Li, K. Li, and L. Fei-Fei, "Imagenet: A large-scale hierarchical image database," in *2009 IEEE Conference on Computer Vision and Pattern Recognition*, 2009, pp. 248–255.
- [7] O. Russakovsky, J. Deng, H. Su, J. Krause, S. Satheesh, S. Ma, Z. Huang, A. Karpathy, A. Khosla, M. Bernstein, A. C. Berg, and L. Fei-Fei, "ImageNet Large Scale Visual Recognition Challenge," *International Journal of Computer Vision (IJCV)*, vol. 115, no. 3, pp. 211–252, 2015.
- [8] T.-Y. Lin, M. Maire, S. Belongie, J. Hays, P. Perona, D. Ramanan, P. Dollár, and C. L. Zitnick, "Microsoft coco: Common objects in context," in *Computer Vision—ECCV 2014: 13th European Conference, Zurich, Switzerland, September 6–12, 2014, Proceedings, Part V 13*. Springer, 2014, pp. 740–755.
- [9] C. L. P. Chen and Z. Liu, "Broad learning system: An effective and efficient incremental learning system without the need for deep architecture," *IEEE Transactions on Neural Networks and Learning Systems*, vol. 29, no. 1, pp. 10–24, 2018.

- [10] J. Lin, G. Han, X. Pan, Z. Liu, H. Chen, D. Li, X. Jia, Z. Shi, Z. Wang, Y. Cui, H. Li, C. Liang, L. Liang, Y. Wang, and C. Han, "Pdbl: Improving histopathological tissue classification with plug-and-play pyramidal deep-broad learning," *IEEE Transactions on Medical Imaging*, vol. 41, no. 9, pp. 2252–2262, 2022.
- [11] J. Choe and H. Shim, "Attention-based dropout layer for weakly supervised object localization," in *2019 IEEE/CVF Conference on Computer Vision and Pattern Recognition (CVPR)*, 2019, pp. 2214–2223.
- [12] C. Han, J. Lin, J. Mai, Y. Wang, Q. Zhang, B. Zhao, X. Chen, X. Pan, Z. Shi, Z. Xu, S. Yao, L. Yan, H. Lin, X. Huang, C. Liang, G. Han, and Z. Liu, "Multi-layer pseudo-supervision for histopathology tissue semantic segmentation using patch-level classification labels," *Medical Image Analysis*, vol. 80, p. 102487, 2022.
- [13] Y. Wang, J. Zhang, M. Kan, S. Shan, and X. Chen, "Self-supervised equivariant attention mechanism for weakly supervised semantic segmentation," in *2020 IEEE/CVF Conference on Computer Vision and Pattern Recognition (CVPR)*, 2020, pp. 12 272–12 281.
- [14] S. Jo and I.-J. Yu, "Puzzle-cam: Improved localization via matching partial and full features," in *2021 IEEE International Conference on Image Processing (ICIP)*, 2021, pp. 639–643.
- [15] P.-T. Jiang, Y. Yang, Q. Hou, and Y. Wei, "L2g: A simple local-to-global knowledge transfer framework for weakly supervised semantic segmentation," in *Proceedings of the IEEE/CVF Conference on Computer Vision and Pattern Recognition (CVPR)*, June 2022, pp. 16 886–16 896.
- [16] J. Fan, Z. Zhang, T. Tan, C. Song, and J. Xiao, "Cian: Cross-image affinity net for weakly supervised semantic segmentation," in *Proceedings of the AAAI Conference on Artificial Intelligence*, 2020.
- [17] J. Lee, E. Kim, S. Lee, J. Lee, and S. Yoon, "Ficklenet: Weakly and semi-supervised semantic image segmentation using stochastic inference," *2019 IEEE/CVF Conference on Computer Vision and Pattern Recognition (CVPR)*, pp. 5262–5271, 2019.
- [18] S. Lee, M. Lee, J. Lee, and H. Shim, "Railroad is not a train: Saliency as pseudo-pixel supervision for weakly supervised semantic segmentation," in *2021 IEEE/CVF Conference on Computer Vision and Pattern Recognition (CVPR)*, 2021, pp. 5491–5501.
- [19] Q. Yao and X. Gong, "Saliency guided self-attention network for weakly and semi-supervised semantic segmentation," *IEEE Access*, vol. 8, pp. 14 413–14 423, 2020.
- [20] X. Zhang, Y. Wei, J. Feng, Y. Yang, and T. Huang, "Adversarial complementary learning for weakly supervised object localization," in *2018 IEEE/CVF Conference on Computer Vision and Pattern Recognition*, 2018, pp. 1325–1334.
- [21] S. Yun, D. Han, S. J. Oh, S. Chun, J. Choe, and Y. Yoo, "Cutmix: Regularization strategy to train strong classifiers with localizable features," in *International Conference on Computer Vision (ICCV)*, 2019.
- [22] L. Zhu, Q. She, Q. Chen, Y. You, B. Wang, and Y. Lu, "Weakly supervised object localization as domain adaption," in *Proceedings of the IEEE/CVF Conference on Computer Vision and Pattern Recognition*, 2022, pp. 14 637–14 646.
- [23] S. Dong, P. Wang, and K. Abbas, "A survey on deep learning and its applications," *Computer Science Review*, vol. 40, p. 100379, 2021.
- [24] S. Gao, Z.-Y. Li, M.-H. Yang, M.-M. Cheng, J. Han, and P. Torr, "Large-scale unsupervised semantic segmentation," *IEEE Transactions on Pattern Analysis and Machine Intelligence*, pp. 1–20, 2022.
- [25] A. Chattopadhyay, A. Sarkar, P. Howlader, and V. N. Balasubramanian, "Grad-cam++: Generalized gradient-based visual explanations for deep convolutional networks," in *2018 IEEE Winter Conference on Applications of Computer Vision (WACV)*, 2018, pp. 839–847.
- [26] D. Omeiza, S. Speakman, C. Cintas, and K. Weldermariam, "Smooth grad-cam++: An enhanced inference level visualization technique for deep convolutional neural network models," *arXiv preprint arXiv:1908.01224*, 2019.
- [27] P.-T. Jiang, C.-B. Zhang, Q. Hou, M.-M. Cheng, and Y. Wei, "Layer-cam: Exploring hierarchical class activation maps for localization," *IEEE Transactions on Image Processing*, vol. 30, pp. 5875–5888, 2021.
- [28] L. Zhu, Q. Chen, L. Jin, Y. You, and Y. Lu, "Bagging regional classification activation maps for weakly supervised object localization," in *Computer Vision – ECCV 2022*, S. Avidan, G. Brostow, M. Cissé, G. M. Farinella, and T. Hassner, Eds. Cham: Springer Nature Switzerland, 2022, pp. 176–192.
- [29] H. Wang, R. Naidu, J. Michael, and S. S. Kundu, "Ss-cam: Smoothed score-cam for sharper visual feature localization," *arXiv preprint arXiv:2006.14255*, 2020.
- [30] R. Naidu, A. Ghosh, Y. Maurya, S. S. Kundu *et al.*, "Is-cam: Integrated score-cam for axiomatic-based explanations," *arXiv preprint arXiv:2010.03023*, 2020.
- [31] S. Desai and H. G. Ramaswamy, "Ablation-cam: Visual explanations for deep convolutional network via gradient-free localization," in *2020 IEEE Winter Conference on Applications of Computer Vision (WACV)*, 2020, pp. 972–980.
- [32] J. R. Lee, S. Kim, I. Park, T. Eo, and D. Hwang, "Relevance-cam: Your model already knows where to look," in *2021 IEEE/CVF Conference on Computer Vision and Pattern Recognition (CVPR)*, 2021, pp. 14 939–14 948.
- [33] Z. Liu and C. L. P. Chen, "Broad learning system: Structural extensions on single-layer and multi-layer neural networks," in *2017 International Conference on Security, Pattern Analysis, and Cybernetics (SPAC)*, 2017, pp. 136–141.
- [34] X. Gong, T. Zhang, C. L. P. Chen, and Z. Liu, "Research review for broad learning system: Algorithms, theory, and applications," *IEEE Transactions on Cybernetics*, vol. 52, no. 9, pp. 8922–8950, 2022.
- [35] S. Feng and C. P. Chen, "Fuzzy broad learning system: A novel neuro-fuzzy model for regression and classification," *IEEE Transactions on Cybernetics*, vol. 50, no. 2, pp. 414–424, 2020.
- [36] J. Lin, Z. Liu, C. Chen, and Y. Zhang, "Three-domain fuzzy wavelet broad learning system for tremor estimation," *Knowledge-Based Systems*, vol. 192, p. 105295, 12 2019.
- [37] Z. Liu, C. L. P. Chen, S. Feng, Q. Feng, and T. Zhang, "Stacked broad learning system: From incremental flatted structure to deep model," *IEEE Transactions on Systems, Man, and Cybernetics: Systems*, vol. 51, no. 1, pp. 209–222, 2021.
- [38] M. Xu, M. Han, C. L. P. Chen, and T. Qiu, "Recurrent broad learning systems for time series prediction," *IEEE Transactions on Cybernetics*, vol. 50, no. 4, pp. 1405–1417, 2020.
- [39] Y. Ma, Z. Liu, and C. L. P. Chen, "Multiscale random convolution broad learning system for hyperspectral image classification," *IEEE Geoscience and Remote Sensing Letters*, vol. 19, pp. 1–5, 2022.
- [40] S. Xu, J. Liu, C. Yang, X. Wu, and T. Xu, "A learning-based stable servo control strategy using broad learning system applied for microrobotic control," *IEEE Transactions on Cybernetics*, vol. 52, no. 12, pp. 13 727–13 737, 2022.
- [41] T. Deng, Y. Huang, Z. Shi, J. Lin, Q. Dou, K. Zhao, F.-F. Liu, Y.-M. Jia, J. Wang, B. Zhao *et al.*, "Feddbl: Communication and data efficient federated deep-broad learning for histopathological tissue classification," *arXiv preprint arXiv:2302.12662*, 2023.
- [42] M. Everingham, S. A. Eslami, L. Van Gool, C. K. Williams, J. Winn, and A. Zisserman, "The pascal visual object classes challenge: A retrospective," *International journal of computer vision*, vol. 111, pp. 98–136, 2015.
- [43] J. Choe, S. J. Oh, S. Lee, S. Chun, Z. Akata, and H. Shim, "Evaluating weakly supervised object localization methods right," in *Conference on Computer Vision and Pattern Recognition (CVPR)*, 2020, to appear.
- [44] J. Choe, S. J. Oh, S. Chun, S. Lee, Z. Akata, and H. Shim, "Evaluation for weakly supervised object localization: Protocol, metrics, and datasets," *IEEE Transactions on Pattern Analysis and Machine Intelligence*, pp. 1–1, 2022.
- [45] M. Amgad, L. A. Atteya, H. Hussein, K. H. Mohammed, E. Hafiz, M. A. T. Elsebaie, A. M. Alhousseiny, M. A. AlMoslemany, A. M. Elmatboly, P. A. Pappalardo, R. A. Sakr, P. Mobadersany, A. Rachid, A. M. Saad, A. M. Alkashash, I. A. Ruhban, A. Alrefai, N. M. Elgazar, A. Abdulkarim, A.-A. Farag, A. Etman, A. G. Elsaed, Y. Alagha, Y. A. Amer, A. M. Raslan, M. K. Nadim, M. A. T. Elsebaie, A. Ayad, L. E. Hanna, A. Gadallah, M. Elkady, B. Drumheller, D. Jaye, D. Manthey, D. A. Gutman, H. Elfandy, and L. A. D. Cooper, "NuCLS: A scalable crowdsourcing approach and dataset for nucleus classification and segmentation in breast cancer," *GigaScience*, vol. 11, 2022.
- [46] R. Benenson, S. Popov, and V. Ferrari, "Large-scale interactive object segmentation with human annotators," in *2019 IEEE/CVF Conference on Computer Vision and Pattern Recognition (CVPR)*, 2019, pp. 11 692–11 701.
- [47] H. Zhang, C. Wu, Z. Zhang, Y. Zhu, H. Lin, Z. Zhang, Y. Sun, T. He, J. Mueller, R. Manmatha *et al.*, "Resnest: Split-attention networks," in *Proceedings of the IEEE/CVF conference on computer vision and pattern recognition*, 2022, pp. 2736–2746.
- [48] Z. Wu, C. Shen, and A. Van Den Hengel, "Wider or deeper: Revisiting the resnet model for visual recognition," *Pattern Recognition*, vol. 90, pp. 119–133, 2019.

- [49] T. Ma and A. Zhang, "Affinitynet: semi-supervised few-shot learning for disease type prediction," in *Proceedings of the AAAI conference on artificial intelligence*, vol. 33, no. 01, 2019, pp. 1069–1076.
- [50] J. Ahn, S. Cho, and S. Kwak, "Weakly supervised learning of instance segmentation with inter-pixel relations," in *Proceedings of the IEEE/CVF conference on computer vision and pattern recognition*, 2019, pp. 2209–2218.